Y. Bazilevs
Department of Structural Engineering,
University of California–San Diego,
La Jolla, CA 92093
e-mail: yuri@ucsd.edu

A. Korobenko
Department of Structural Engineering,
University of California–San Diego,
La Jolla, CA 92093

X. Deng
Department of Structural Engineering,
University of California–San Diego,
La Jolla, CA 92093

J. Yan
Department of Structural Engineering,
University of California–San Diego,
La Jolla, CA 92093

M. Kinzel
Department of Aerospace Engineering,
Division of Engineering and Applied Science,
California Institute of Technology,
Pasadena, CA 91125

J. O. Dabiri
Department of Aerospace Engineering,
Division of Engineering and Applied Science,
California Institute of Technology,
Pasadena, CA 91125

Fluid–Structure Interaction Modeling of Vertical-Axis Wind Turbines

Full-scale, 3D, time-dependent aerodynamics and fluid–structure interaction (FSI) simulations of a Darrieus-type vertical-axis wind turbine (VAWT) are presented. A structural model of the Windspire VAWT (Windspire energy, http://www.windspireenergy.com/) is developed, which makes use of the recently proposed rotation-free Kirchhoff–Love shell and beam/cable formulations. A moving-domain finite-element-based ALE-VMS (arbitrary Lagrangian–Eulerian-variational-multiscale) formulation is employed for the aerodynamics in combination with the sliding-interface formulation to handle the VAWT mechanical components in relative motion. The sliding-interface formulation is augmented to handle nonstationary cylindrical sliding interfaces, which are needed for the FSI modeling of VAWTs. The computational results presented show good agreement with the field-test data. Additionally, several scenarios are considered to investigate the transient VAWT response and the issues related to self-starting. [DOI: 10.1115/1.4027466]

1 Introduction

In recent years, the wind-energy industry has been moving in two main directions: off shore, where energy can be harvested from stronger and more sustained winds, and urban areas, which are closer to the direct consumer. In the offshore environments, large-size horizontal-axis wind turbines (HAWTs) are at the leading edge. They are equipped with complicated pitch and yaw control mechanisms to keep the turbine in operation for wind velocities of variable magnitude and direction, such as wind gusts. The existing HAWT designs are currently more efficient for large-scale power production compared with the VAWT designs. However, smaller-size VAWTs are more suitable for urban environments and are currently employed for small-scale wind-energy generation. Nevertheless, wind-energy technologies are maturing, and several studies were recently initiated that involve placing VAWTs off shore [2,3].

There are two main configurations of VAWTs, employing the Savonius or Darrieus rotor types [4]. The Darrieus configuration is a lift-driven turbine. It is more efficient than the Savonius configuration, which is a drag-type design. Recently, VAWTs resurfaced as a good source of small-scale electric power for urban areas. The main reason for this is their compact design. The generator and drive train components are located close to the ground, which allows for easier installation, maintenance, and repair. Another advantage of VAWTs is that they are omidirectional (i.e., they do not have to be oriented into the main wind direction), which obviates the need to include expensive yaw control mechanisms in their design. However, this brings up issues related to self-starting. The ability of VAWTs to self-start depends on the wind conditions as well as on airfoil designs employed [5]. Studies in Refs. [6,7] reported that a three-bladed H-type Darrieus rotor using a symmetric airfoil is able to self-start. In Ref. [8], the author showed that significant atmospheric wind transients are required to complete the self-starting process for a fixed-blade Darieus turbine when it is initially positioned in a dead-band region defined as the region with the tip-speed-ratio values that result in negative net energy produced per cycle. Self-starting remains an open issue for VAWTs, and an additional starting system is often required for successful operation.

Due to increased recent emphasis on renewable energy, and, in particular, wind energy, aerodynamics modeling and simulation of HAWTs in 3D have become a popular research activity [9–17]. FSI modeling of HAWTs is less developed, although, recently, several studies were reported showing validation at full-scale against field-test data for medium-size turbines [18], and demonstrating feasibility for application to larger-size offshore wind-turbine designs [10,19]. However, 3D aerodynamics modeling of VAWTs is lagging behind. The majority of the computations for VAWTs are reported in 2D [20–22], while a recent 3D simulation in Ref. [23] employed a quasi-static representation of the air flow instead of solving the time-dependent problem. A detailed 3D aerodynamics analysis of a VAWT used for laboratory testing was recently performed by some of the authors of the present paper in Ref. [24]. The studies included full 3D aerodynamic simulations, validated using experimental data, and a simulation of two side-by-site counter-rotating turbines.

The aerodynamics and FSI computational challenges in VAWTs are different than in HAWTs due to the differences in their aerodynamic and structural design. Because the rotation axis

Manuscript received March 25, 2014; final manuscript received April 14, 2014; accepted manuscript posted April 22, 2014; published online May 7, 2014. Assoc. Editor: Kenji Takizawa.

is orthogonal to the wind direction, the wind-turbine blades experience rapid and large variations in the angle of attack resulting in an air flow that is constantly switching from being fully attached to being fully separated. This, in turn, leads to high-frequency and high-amplitude variations in the aerodynamic torque acting on the rotor, requiring finer mesh resolution and smaller time-step size for accurate simulation [24]. VAWT blades are typically long and slender by design. The ratio of cord length to blade height is very low, requiring finer mesh resolution also in the blade height direction in order to avoid using high-aspect-ratio surface elements, and to better capture turbulent fluctuations in the boundary layer. When the FSI analysis of VAWTs is performed, the simulation complexity is further increased. The flexibility in VAWTs does not come from the blades, which are practically rigid (although blades deform at high rotational speeds), but rather from the tower itself, and its connection to the rotor and ground. As a result, the main FSI challenge is to be able to simulate a spinning rotor that is mounted on a flexible tower.

In the present paper, we focus on the following developments. We propose a set of techniques that, for the first time, enable FSI simulations of VAWTs in 3D and at full-scale. We first develop a 3D structural model of a Windspire VAWT [1], which makes use of the recently proposed rotation-free Kirchhoff–Love shell and beam/cable formulations, and their coupling. The model allows for the rotor to spin freely and for the tower and blades to undergo elastic deformations. We validate the aerodynamics of the Windspire design using the field data reported in Refs. [25–27]. For the FSI computations, to accommodate the spinning rotor and deflecting tower and blades, the FSI formulation from Ref. [19] is enhanced to allow the cylindrical sliding interface to also move in space. Finally, with these new techniques, we perform preliminary FSI computations in an effort to better understand the self-starting issues.

The paper is outlined as follows. In Sec. 2, we introduce the FSI formulation and present the governing equations of aerodynamics and structural mechanics. We also briefly describe the discretization techniques employed and the aforementioned enhancement of the sliding-interface formulation. In Sec. 3, we show the aerodynamic and FSI computations of the Windspire VAWT and discuss start-up issues. In Sec. 4, we draw conclusions and discuss possible future research directions.

2 Methods for Modeling and Simulation of VAWTs

2.1 Governing Equations at the Continuum Level. To perform the VAWT simulations, we adopt the FSI framework developed in Ref. [28]. The wind turbine aerodynamics is governed by the Navier–Stokes equations of incompressible flows. The incompressible-flow assumption is valid for the present application because the Mach number is low (≈ 0.1). The Navier–Stokes equations are posed on a moving spatial domain and are written in the ALE frame [29] as follows:

$$\rho_1\left(\left.\frac{\partial \mathbf{u}}{\partial t}\right|_{\hat{x}} + (\mathbf{u}-\hat{\mathbf{u}})\cdot\nabla\mathbf{u} - \mathbf{f}_1\right) - \nabla\cdot\boldsymbol{\sigma}_1 = \mathbf{0} \tag{1}$$

$$\nabla\cdot\mathbf{u} = 0 \tag{2}$$

where ρ_1 is the fluid density, $\mathbf{f}_1$ is the external force per unit mass, $\mathbf{u}$ and $\hat{\mathbf{u}}$ are velocities of the fluid and fluid mechanics domain, respectively. The stress tensor $\boldsymbol{\sigma}_1$ is defined as

$$\boldsymbol{\sigma}_1(\mathbf{u},p) = -p\mathbf{I} + 2\mu\boldsymbol{\varepsilon}(\mathbf{u}) \tag{3}$$

where p is the pressure, $\mathbf{I}$ is the identity tensor, μ is the dynamic viscosity, and $\boldsymbol{\varepsilon}(\mathbf{u})$ is the strain-rate tensor given by

$$\boldsymbol{\varepsilon}(\mathbf{u}) = \frac{1}{2}\left(\nabla\mathbf{u} + \nabla\mathbf{u}^T\right) \tag{4}$$

In Eq. (1), $|_{\hat{x}}$ denotes the time derivative taken with respect to a fixed referential domain spatial coordinates $\hat{\mathbf{x}}$. The spatial derivatives in the above equations are taken with respect to the spatial coordinates $\mathbf{x}$ of the current configuration.

The governing equations of structural mechanics written in the Lagrangian frame [30] consist of the local balance of linear momentum, and are given by

$$\rho_2\left(\frac{\mathrm{d}^2\mathbf{y}}{\mathrm{d}t^2} - \mathbf{f}_2\right) - \nabla\cdot\boldsymbol{\sigma}_2 = \mathbf{0} \tag{5}$$

where ρ_2 is the structural density, $\mathbf{f}_2$ is the body force per unit mass, $\boldsymbol{\sigma}_2$ is the structural Cauchy stress, and $\mathbf{y}$ is the unknown structural displacement vector.

At the fluid–structure interface, compatibility of the kinematics and tractions is enforced, namely

$$\mathbf{u} - \frac{\mathrm{d}\mathbf{y}}{\mathrm{d}t} = \mathbf{0} \tag{6}$$

$$\boldsymbol{\sigma}_1\mathbf{n}_1 + \boldsymbol{\sigma}_2\mathbf{n}_2 = \mathbf{0} \tag{7}$$

where $\mathbf{n}_1$ and $\mathbf{n}_2$ are the unit outward normal vectors to the fluid and structural mechanics domain at their interface. Note that $\mathbf{n}_1 = -\mathbf{n}_2$.

The above equations constitute the basic formulation of the FSI problem at the continuous level. In what follows, we discuss the discretization of the above system that is applicable to VAWT modeling. For a variety of discretization options, FSI coupling strategies, and applications to a large class of problems in engineering, the reader is referred to the recent book on computational FSI [31].

2.2 Discretization and Special FSI Techniques for VAWTs. The aerodynamics formulation makes use of the FEM-based ALE-VMS approach [29,32,33] augmented with weakly enforced boundary conditions [34–36]. The former acts as a turbulence model, while the latter relaxes the mesh size requirements in the boundary layer without sacrificing the solution accuracy. ALE-VMS was successfully employed for the aerodynamics simulation of HAWTs and VAWTs in Refs. [9,16,24,37,38], and fluid–structure interaction simulation of HAWTs in Refs. [10,18,19,28].

The structural mechanics of VAWTs are modeled using a combination of the recently proposed displacement-based Kirchhoff–Love shell [10,18,39] and beam/cable [40] formulations. Both are discretized using NURBS-based isogeometric analysis (IGA) [41,42].

The FSI modeling employed here makes use of nonmatching discretization of the interface between the fluid and structure subdomains. Nonmatching discretizations at the fluid–structure interface require the use of interpolation or projection of kinematic and traction data between the nonmatching surface meshes (see, for example, Refs. [28,31,32,43–52]), which is what we do here.

To handle the rotor motion in the aerodynamics problem, the sliding-interface approach is employed. The sliding-interface formulation was developed in Ref. [53] to handle flows about objects in relative motion, and used in the computation of HAWTs in Ref. [16], including FSI coupling [19], and VAWTs in Ref. [24]. We note that in application of the FEM to flows with moving mechanical components, alternatively to the sliding-interface approach, the Shear–Slip Mesh Update Method [54–56] and its more general versions [57,58] may also be used to handle objects in relative motion. A recently developed set of space-time (ST) methods can serve as a third alternative in dealing with objects in relative motion. The components of this set include the ST/NURBS mesh update method [17,59,60], ST interface tracking with topology change [61], and ST computation technique with continuous representation in time [62].

To accommodate the spinning motion of the rotor superposed on the global elastic deformation of the VAWT, and to maintain a

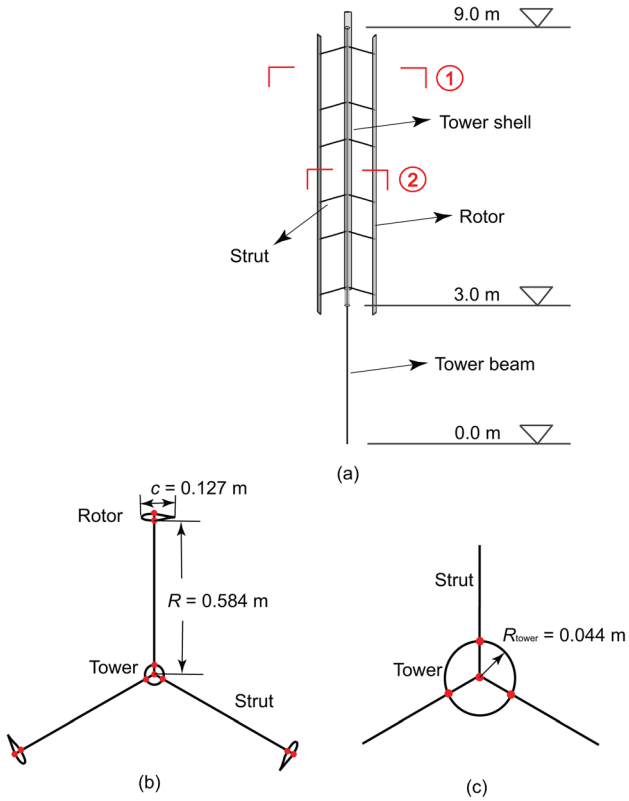

Fig. 1 Windspire VAWT structural model with dimensions included: (*a*) full model using isogeometric NURBS-based rotation-free shells and beams; (*b*) model cross section 1 showing attachment of the struts to the blades and tower shell; (*c*) model cross section 2 showing attachment of the struts and tower shell

Table 1 Geometric and material properties of the main VAWT structural components

Part	Thickness/ radius t/r (mm)	Young's modulus E (GPa)	Poisson's ratio ν	Density ρ (kg/m^3)
Blades	2/NA	70	0.35	2700
Strut	12.7/NA	70	0.35	2700
Tower shell	5/44.45	210	0.33	78
Tower beam	NA/41.08	210	NA	5120.9

Table 2 Masses of the main VAWT structural components

Part	Mass (kg)
Blades	26.3
Strut	14.1
Tower	243.4
Total	283.8

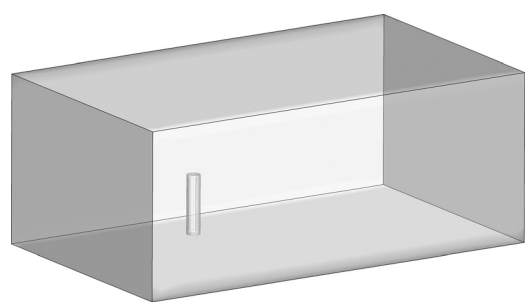

Fig. 2 The VAWT aerodynamics computational domain in the reference configuration, including the inner cylindrical region, outer region, and sliding interface that is now allowed to move in space as a rigid object

moving-mesh discretization with good boundary-layer resolution critical for aerodynamics accuracy, the sliding-interface technique is "upgraded" to handle more complex structural motions. While at the fluid–structure interface the fluid mechanics mesh follows the rotor motion, the outer boundary of the cylindrical domain that encloses the rotor is only allowed to move as a rigid object. The rigid-body motion part is extracted from the rotor structural mechanics solution (see, e.g., Ref. [63]) and is applied directly to the outer boundary of the cylindrical domain enclosing the rotor. The inner boundary of the domain that encloses the cylindrical subdomain also moves as a rigid object. It follows the motion of the cylindrical subdomain, but with the spinning component of the motion removed. The fluid mechanics mesh motion in the interior of the two subdomains is governed by the equations of elastostatics with Jacobian-based stiffening [43,57,64–67] to preserve the aerodynamic mesh quality.

3 Computational Results

The computations presented in this section are performed for a 1.2 kW Windspire design [1], a three-bladed Darrieus VAWT. The total height of the VAWT tower is 9.0 m and the rotor height is 6.0 m. The rotor uses the DU06W200 airfoil profile with the chord length of 0.127 m, and is of the Giromill type with straight vertical blade sections attached to the main shaft with horizontal struts (see Fig. 1). The blades and struts are made of aluminum, and the tower is made of steel. The material parameters and masses of the main structural components are given in Tables 1 and 2.

The VAWT blades and part of the tower that spins with the rotor are modeled using Kirchhoff–Love shells, while the struts and main shaft are modeled as beams. The struts are connected to the blades, tower shell, and main shaft, which gives a relatively simple VAWT structural model that can represent the 3D mechanics of a spinning, flexible rotor mounted on a flexible tower. See Figs. 1(*b*) and 1(*c*) for more details of the VAWT geometry description. The density of the tower shell is set to be very small (see Table 1) so that most of tower mass is distributed evenly along the beam. Quadratic NURBS are employed for both the beam and shell discretizations. The total number of beam elements is 116, and total number of shell elements is 7029. We note that all the aerodynamically important surfaces that are "seen" by the fluid mechanics discretization are modeled using shells.

The aerodynamics and FSI simulations are carried out at realistic operating conditions reported in the field-test experiments conducted by the National Renewable Energy Laboratory [25] and Caltech Field Laboratory for Optimized Wind Energy [26,27]. For all cases, the air density and viscosity are set to 1.23 kg/m^3 and 1.78×10^{-5} kg/ms, respectively.

The outer aerodynamics computational domain has the dimensions of 50 m, 20 m, and 30 m in the streamwise, vertical, and spanwise directions, respectively, and is shown in Fig. 2. The VAWT centerline is located 15 m from the inflow and side boundaries. The radius and height of the inner cylindrical domain that encloses the rotor are 1.6 m and 7 m, respectively.

At the inflow, a uniform wind velocity profile is prescribed. On the top, bottom, and side surfaces of the outer domain no-penetration boundary conditions are prescribed, while zero traction boundary conditions are set at the outflow.

The aerodynamics mesh has about 8 M elements, which are linear triangular prisms in the blade boundary layers, and linear tetrahedra elsewhere. The boundary-layer mesh is constructed using 18 layers of elements, with the size of the first element in the

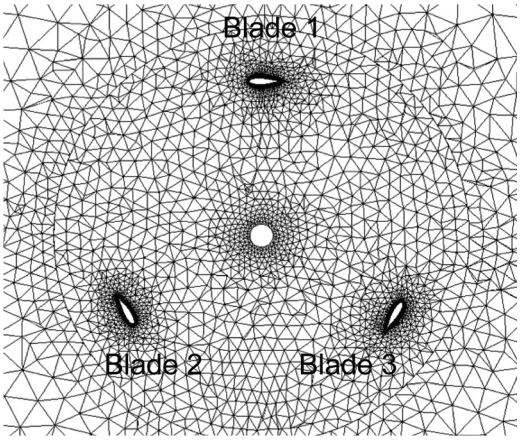

Fig. 3 A 2D cross section of the computational mesh along the rotor axis. The view is from the top of the turbine, and the blades are numbered counterclockwise, which is the expected direction of rotation. The sliding interface may be seen along a circular curve where the mesh appears to be nonconforming.

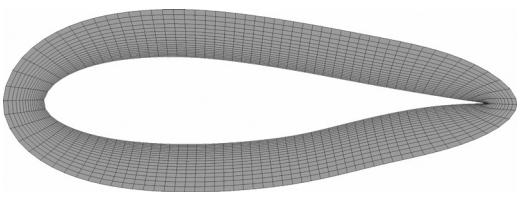

Fig. 4 A 2D cross section of the blade boundary-layer mesh consisting of triangular prisms

wall-normal direction of 0.0003 m, and growth ratio of 1.1. A 2D slice of the mesh near the rotor is shown in Fig. 3, while Fig. 4 shows the zoom on the boundary-layer mesh near one of the blades. The mesh design employed in this simulation is based on a refinement study performed for a Darrieus-type experimental turbine in Ref. [24].

All computations are carried out in a parallel computing environment. The mesh is partitioned into subdomains using METIS [68], and each subdomain is assigned to a compute core. The parallel implementation of the methodology may be found in Ref. [37]. The time-step is set to 1.0×10^{-5} s for the aerodynamics computation and 2.0×10^{-5} s for the FSI analysis.

3.1 Aerodynamics Simulation of the Windspire VAWT. We first performed two pure aerodynamic simulations of the Windspire VAWT, one using the wind speed of 8.0 m/s and rotor speed of 32.7 rad/s, and another using the wind speed of 6.0 m/s and rotor speed of 20.6 rad/s. The time history of the aerodynamic torque for both cases is plotted in Fig. 5 together with the experimental values reported from field-test experiments [25–27]. After the rotor undergoes a full revolution, a nearly periodic solution is attained in both cases. For 8.0 m/s wind, the predicted average torque is 18.9 Nm, while its experimentally reported value is about 12.7 Nm. For 6.0 m/s wind, the predicted average torque is 9.5 Nm, while its experimentally reported value is about 4.8 Nm.

In both cases, the experimental value of the aerodynamic torque is derived from the average power produced by the turbine at the target rotor speed. The difference in the predicted and experimentally reported aerodynamic torque is likely due to the mechanical and electrical losses in the system, which are not reported. To estimate those, we perform the following analysis. For simplicity, we assume that the torque loss is proportional to the rotational speed of the turbine, that is

$$T_{\text{loss}} = c_{\text{loss}}\dot{\theta} \tag{8}$$

Here, T_{loss} is taken as the difference between the predicted and reported torque values, $\dot{\theta}$ is the rotation speed, and c_{loss} is the "loss" constant that characterizes the turbine. The data for the 8.0 m/s wind give $c_{\text{loss}} = 0.19$ kg m^2/rad, while for 6.0 m/s wind we find that $c_{\text{loss}} = 0.23$ kg m^2/rad. The two values are reasonably close, which suggests that the torque overestimation is consistent with the loss model. In fact, this technique of combining experimental measurements and advanced computation may be employed to approximately estimate losses in wind turbines.

3.2 FSI Simulations of the Windspire VAWT. In this section, we perform a preliminary investigation of the start-up issues in VAWTs using the FSI methodology described earlier and the structural model of the Windspire design. We fix the inflow wind speed at 11.4 m/s, and consider three initial rotor speeds: 0 rad/s, 4 rad/s, and 12 rad/s. Of interest is the transient response of the system. In particular, we will focus on how the rotor angular speed responds to the prescribed initial conditions, and what is the range of the tower tip displacement during the VAWT operation.

The starting configuration of the VAWT is shown in Fig. 3. Blade 1 is placed parallel to the flow with the airfoil leading edge facing the wind. Blades 2 and 3 are placed at an angle to the flow

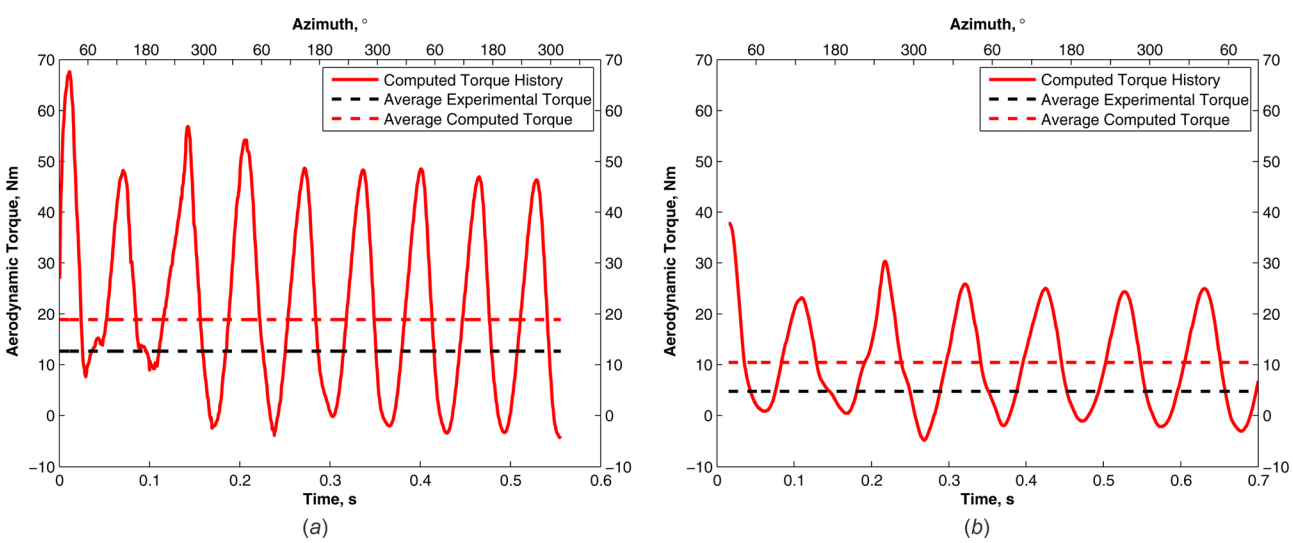

Fig. 5 Time history of the aerodynamic torque for the pure aerodynamics simulations. (*a*) 8.0 m/s wind with experimental data from Ref. [25] and (*b*) 6.0 m/s wind with experimental data from Refs. [26,27].

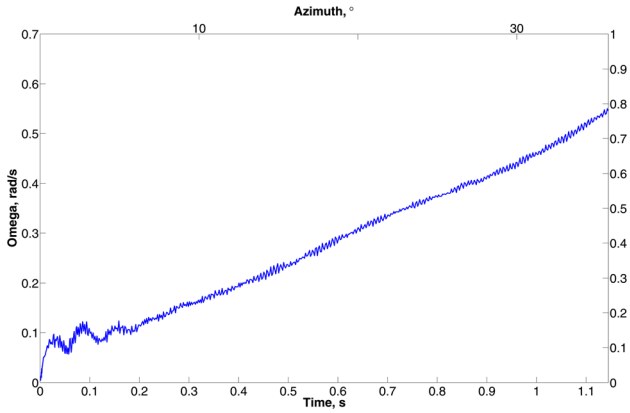

Fig. 6 Time history of the rotor speed starting from 0 rad/s

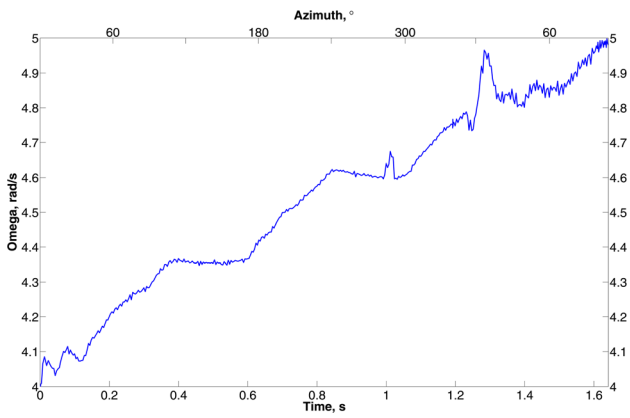

Fig. 7 Time history of the rotor speed starting from 4 rad/s

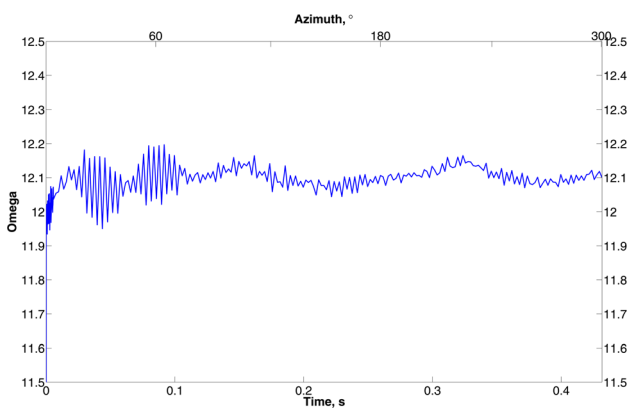

Fig. 8 Time history of the rotor speed starting from 12 rad/s

with the trailing edge facing the wind. (Blade numbering is shown in the figure.)

The time history of rotor speed is shown in Figs. 6–8. For the 0 rad/s case, the rotor speed begins to increase suggesting this configuration is favorable for self-starting. For the 4 rad/s case, the rotor speed has a nearly linear acceleration region followed by a *plateau* region. In Ref. [7], the plateau region is defined as the regime when the turbine operates at nearly constant (i.e., steady-state like) rotational speed. From the angular position of the blades in Fig. 7, it is evident that the plateau region occurs approximately every 120 deg when one of the blades is in a stalled position. It lasts until the blade clears the stalled region, and the lift forces are sufficiently high for the rotational speed to start

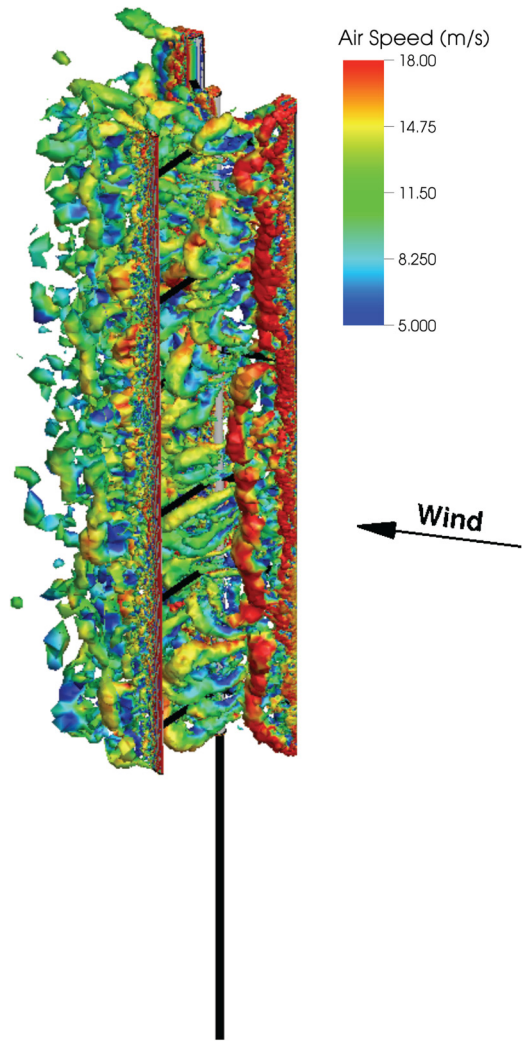

Fig. 9 Vorticity isosurfaces at a time instant colored by velocity magnitude for the 4 rad/s case

increasing again. As the rotational speed increases, the angular velocity is starting to exhibit local unsteady behavior in the plateau region. While the overall growth of the angular velocity for the 4 rad/s case is promising for the VAWT to self-start, the situation is different for the 12 rad/s case (see Fig. 8). Here, the rotor speed has little dependence on the angular position and stays nearly constant, close to its initial value. It is not likely that the rotor speed will reach to the operational levels in these conditions without an applied external torque, or a sudden change in wind speed, which is consistent with the findings of Ref. [8].

Figure 9 shows, for a full turbine, a snapshot of vorticity colored by flow speed for the 4 rad/s case. Figure 10 zooms on the rotor and shows several flow vorticity snapshots during the rotation cycle. The figures indicate the complexity of the underlying flow phenomena and the associated computational challenges. Note the presence of quasi-2D vortex tubes that are created due to massive flow separation, and that quickly disintegrate and turn into fine-grained 3D turbulence further downstream. For more discussion on the aerodynamics phenomena involved in VAWTs the reader is referred to Ref. [24].

Figure 11 shows the turbine current configuration at two time instances during the cycle for the 4 rad/s case. The displacement is mostly in the direction of the wind, however, lateral tower displacements are also observed as a result of the rotor spinning motion. The displacement amplitude is around 0.10–0.12 m, which is also the case for the 0 rad/s and 12 rad/s cases.

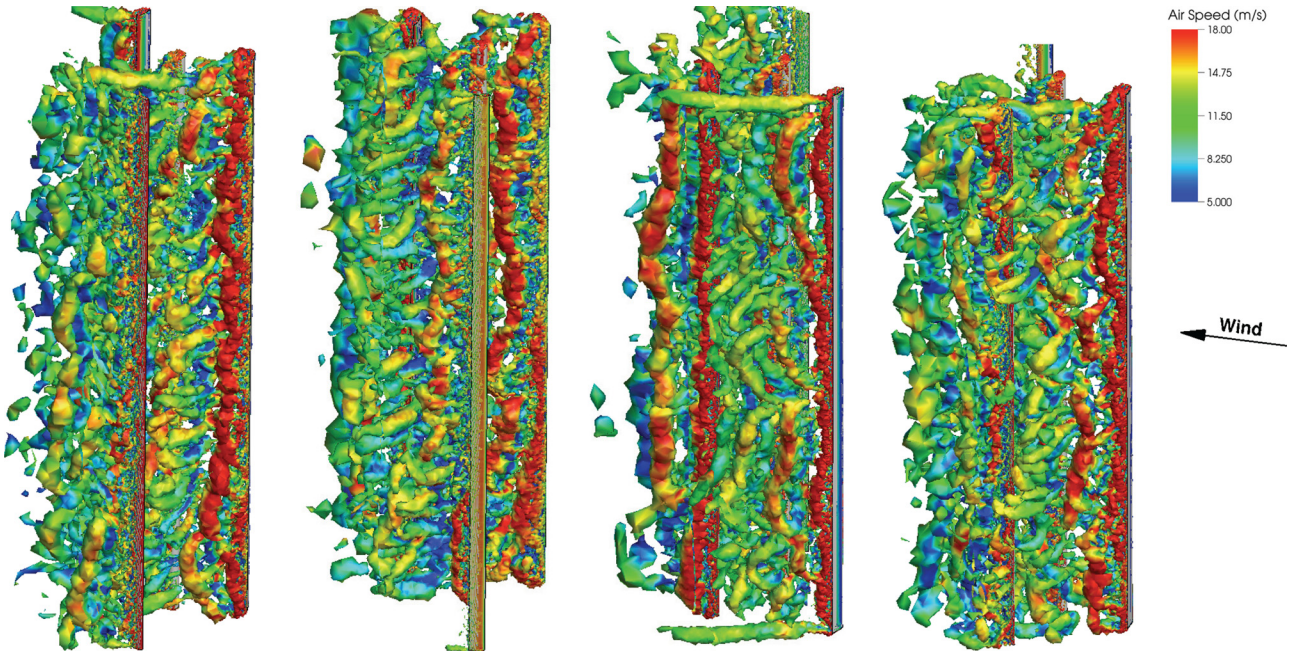

Fig. 10 Vorticity isosurfaces of vorticity colored by velocity magnitude for the 4 rad/s case. Zoom on the rotor. From left to right: vorticity at 1.12 s, 1.24 s, 1.40 s, and 1.50 s.

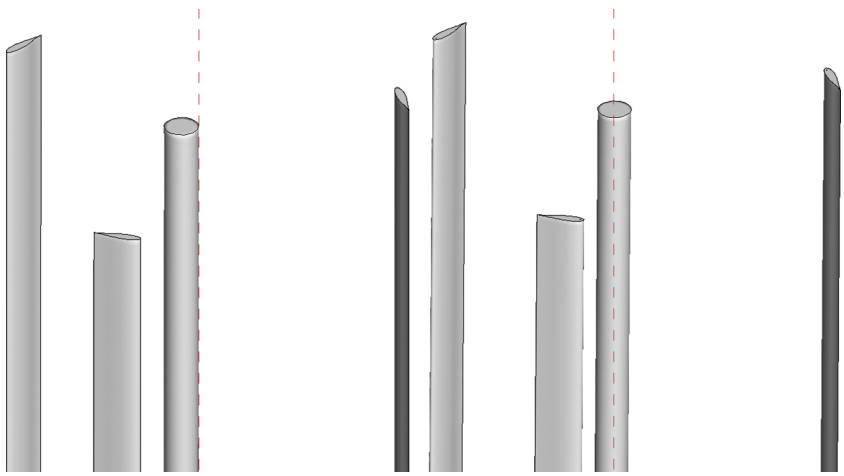

Fig. 11 Turbine current configuration at two time instances for the 4 rad/s case. The tower centerline in the reference configuration is shown using the dashed line to illustrate the range of turbine motion during the cycle. The range of the tower tip displacement during the cycle is about 0.10–0.12 m.

4 Conclusions and Future Work

In this paper, dynamic FSI modeling of VAWTs in 3D and at full-scale was reported for the first time. A structural model of a Windspire wind turbine design was constructed and discretized using the recently proposed isogeometric rotation-free shell and beam formulations. This approach presents a good combination of accuracy due to the structural geometry representation using smooth, higher-order functions, and efficiency due to the fact that only displacement degrees of freedom are employed in the formulation. The ALE-VMS technique for aerodynamics modeling was augmented with an improved version of the sliding-interface formulation, which allows the interface to move in space as a rigid object and accommodate the global turbine deflections in addition to the rotor spinning motion. The pure aerodynamics computation produced good agreement with the field-test data for the Windspire turbine, and the FSI simulations were performed to investigate turbine start-up issues.

From the FSI computations, we see that for given wind conditions, the rotor naturally accelerates at lower values of angular speed. However, as the angular speed grows, the rotor may encounter a dead-band region. That is, the turbine self-starts, but then it is trapped in a lower rotational speed than is required for optimal performance, and some additional input (e.g., a wind gust or applied external torque) is required to get the rotor to accelerate further. There may be multiple dead-band regions that the turbine needs to overcome, with external forcing applied before it reaches the target rotational speed. In the future, to address some of these issues, we plan to couple our FSI formulation with an appropriate control strategy (see, e.g., Ref. [69]) to simulate more realistic VAWT operation scenarios.

Acknowledgment

This work was supported through the NSF CAREER Award No. 1055091. The computational resources of the Texas

Advanced Computing Center (TACC) [70] were employed for the simulations reported in this work. This support is gratefully acknowledged.

References

[1] "Windspire Vertical Wind Turbine," 2014, Ark Alloy, LLC, Reedsburg, WI, http://www.windspireenergy.com/

[2] Vita, L., Paulsen, U. S., and Pedersen, T. F., 2010, "A Novel Floating Offshore Wind Turbine Concept: New Developments," European Wind Energy Conference & Exhibition (EWEC 2010), Warsaw, Poland, April 20–23.

[3] Vita, L., Paulsen, U. S., Madsen, H. A., Nielsen, H. P., Berthelsen, P. A., and Cartsensen, S., 2012, "Design and Aero-Elastic Simulation of a 5 MW Floating Vertical Axis Wind Turbine," ASME Paper No. OMAE2012-83470.

[4] Hau, E., 2006, *Wind Turbines: Fundamentals, Technologies, Application, Economics*, 2nd ed., Springer, Berlin.

[5] Kirke, B., and Lazauskas, L., 1991, "Enhancing the Performance of a Vertical Axis Wind Turbine Using a Simple Variable Pitch System," Wind Eng., **15**(4), pp. 187–195.

[6] Dominy, R., Lunt, P., Bickerdyke, A., and Dominy, J., 2007, "Self-Starting Capability of a Darrieus Turbine," Proc. Inst. Mech. Eng., Part A, **221**(1), pp. 111–120.

[7] Hill, N., Dominy, R., Ingram, G., and Dominy, J., 2009, "Darrieus Turbines: The Physics of Self-Starting," Proc. Inst. Mech. Eng., Part A, **223**(1), pp. 21–29.

[8] Baker, J. R., 1983, "Features to Aid or Enable Self Starting of Fixed Pitch Low Solidity Vertical Axis Wind Turbines," J. Wind Eng. Ind. Aerodyn., **15**(1–3), pp. 369–380.

[9] Bazilevs, Y., Hsu, M.-C., Akkerman, I., Wright, S., Takizawa, K., Henicke, B., Spielman, T., and Tezduyar, T. E., 2011, "3D Simulation of Wind Turbine Rotors at Full Scale. Part I: Geometry Modeling and Aerodynamics," Int. J. Numer. Methods Fluids, **65**(1–3), pp. 207–235.

[10] Bazilevs, Y., Hsu, M.-C., Kiendl, J., Wüchner, R., and Bletzinger, K.-U., 2011, "3D Simulation of Wind Turbine Rotors at Full Scale. Part II: Fluid–Structure Interaction Modeling With Composite Blades," Int. J. Numer. Methods Fluids, **65**(1–3), pp. 236–253.

[11] Chow, R., and van Dam, C. P., 2012, "Verification of Computational Simulations of the NREL 5 MW Rotor With a Focus on Inboard Flow Separation," Wind Energy, **15**(8), pp. 967–981.

[12] Bechmann, A., Sørensen, N. N., and Zahle, F., 2011, "CFD Simulations of the MEXICO Rotor," Wind Energy, **14**(5), pp. 677–689.

[13] Takizawa, K., Henicke, B., Tezduyar, T. E., Hsu, M.-C., and Bazilevs, Y., 2011, "Stabilized Space–Time Computation of Wind-Turbine Rotor Aerodynamics," Comput. Mech., **48**(3), pp. 333–344.

[14] Takizawa, K., Henicke, B., Montes, D., Tezduyar, T. E., Hsu, M.-C., and Bazilevs, Y., 2011, "Numerical-Performance Studies for the Stabilized Space–Time Computation of Wind-Turbine Rotor Aerodynamics," Comput. Mech., **48**(6), pp. 647–657.

[15] Sørensen, N. N., and Schreck, S., 2012, "Computation of the National Renewable Energy Laboratory Phase-VI Rotor in Pitch Motion During Standstill," Wind Energy, **15**(3), pp. 425–442.

[16] Hsu, M.-C., Akkerman, I., and Bazilevs, Y., 2013, "Finite Element Simulation of Wind Turbine Aerodynamics: Validation Study Using NREL Phase VI Experiment," Wind Energy, **17**(3), pp. 461–481.

[17] Takizawa, K., Tezduyar, T. E., McIntyre, S., Kostov, N., Kolesar, R., and Habluetzel, C., 2014, "Space–Time VMS Computation of Wind-Turbine Rotor and Tower Aerodynamics," Comput. Mech., **53**(1), pp. 1–15.

[18] Korobenko, A., Hsu, M., Akkerman, I., Tippmann, J., and Bazilevs, Y., 2013, "Structural Mechanics Modeling and FSI Simulation of Wind Turbines," Math. Models Methods Appl. Sci., **23**(2), pp. 249–272.

[19] Hsu, M.-C., and Bazilevs, Y., 2012, "Fluid–Structure Interaction Modeling of Wind Turbines: Simulating the Full Machine," Comput. Mech., **50**(6), pp. 821–833.

[20] Stein, P., Hsu, M.-C., Bazilevs, Y., and Beucke, K., 2012, "Operator- and Template-Based Modeling of Solid Geometry for Isogeometric Analysis With Application to Vertical Axis Wind Turbine Simulation," Comput. Methods Appl. Mech. Eng., **213–216**, pp. 71–83.

[21] Scheurich, F., Fletcher, T., and Brown, R., 2011, "Simulating the Aerodynamic Performance and Wake Dynamics of a Vertical-Axis Wind Turbine," Wind Energy, **14**(2), pp. 159–177.

[22] Scheurich, F., and Brown, R., 2012, "Modelling the Aerodynamics of Vertical-Axis Wind Turbines in Unsteady Wind Conditions". Wind Energy., **16**(1), pp. 91–107.

[23] McLaren, K., Tullis, S., and Ziada, S., 2012, "Computational Fluid Dynamics Simulation of the Aerodynamics of a High Solidity, Small-Scale Vertical Axis Wind Turbine," Wind Energy, **15**(3), pp. 349–361.

[24] Korobenko, A., Hsu, M.-C., Akkerman, I., and Bazilevs, Y., 2013, "Aerodynamic Simulation of Vertical-Axis Wind Turbines," ASME J. Appl. Mech., **81**(2), p. 021011.

[25] Huskey, A., Bowen, A., and Jager, D., 2009, "Wind Turbine Generator System Power Performance Test Report for the Mariah Windspire 1-kW Wind Turbine," National Renewable Energy Laboratory, Golden, CO, Technical Report No. NREL/TP-500-46192.

[26] Dabiri, J. O., 2011, "Potential Order-of-Magnitude Enhancement of Wind Farm Power Density Via Counter-Rotating Vertical-Axis Wind Turbine Arrays," J. Renewable Sustainable Energy, **3**(4), p. 043104.

[27] "Biological Propulsion Laboratory at CALTECH (Wind Energy Research)," 2012, California Institute of Technology, Pasadena, CA, http://dabiri.caltech.edu/research/wind-energy.html

[28] Bazilevs, Y., Hsu, M.-C., and Scott, M. A., 2012, "Isogeometric Fluid–Structure Interaction Analysis With Emphasis on Non-Matching Discretizations, and With Application to Wind Turbines," Comput. Methods Appl. Mech. Eng., **249–252**, pp. 28–41.

[29] Hughes, T. J. R., Liu, W. K., and Zimmermann, T. K., 1981, "Lagrangian–Eulerian Finite Element Formulation for Incompressible Viscous Flows," Comput. Methods Appl. Mech. Eng., **29**(3), pp. 329–349.

[30] Belytschko, T., Liu, W. K., and Moran, B., 2000, *Nonlinear Finite Elements for Continua and Structures*, Wiley, New York.

[31] Bazilevs, Y., Takizawa, K., and Tezduyar, T. E., 2013, *Computational Fluid–Structure Interaction: Methods and Applications*, Wiley, New York.

[32] Takizawa, K., Bazilevs, Y., and Tezduyar, T. E., 2012, "Space–Time and ALE-VMS Techniques for Patient-Specific Cardiovascular Fluid–Structure Interaction Modeling," Arch. Comput. Methods Eng., **19**(2), pp. 171–225.

[33] Bazilevs, Y., Hsu, M.-C., Takizawa, K., and Tezduyar, T. E., 2012, "ALE-VMS and ST-VMS Methods for Computer Modeling of Wind-Turbine Rotor Aerodynamics and Fluid–Structure Interaction," Math. Models Methods Appl. Sci., **22**(Supp 02), p. 1230002.

[34] Bazilevs, Y., and Hughes, T. J. R., 2007, "Weak Imposition of Dirichlet Boundary Conditions in Fluid Mechanics," Comput. Fluids, **36**(1), pp. 12–26.

[35] Bazilevs, Y., Michler, C., Calo, V. M., and Hughes, T. J. R., 2007, "Weak Dirichlet Boundary Conditions for Wall-Bounded Turbulent Flows," Comput. Methods Appl. Mech. Eng., **196**(49–52), pp. 4853–4862.

[36] Bazilevs, Y., Michler, C., Calo, V. M., and Hughes, T. J. R., 2010, "Isogeometric Variational Multiscale Modeling of Wall-Bounded Turbulent Flows With Weakly Enforced Boundary Conditions on Unstretched Meshes," Comput. Methods Appl. Mech. Eng., **199**(13–16), pp. 780–790.

[37] Hsu, M.-C., Akkerman, I., and Bazilevs, Y., 2011, "High-Performance Computing of Wind Turbine Aerodynamics Using Isogeometric Analysis," Comput. Fluids, **49**(1), pp. 93–100.

[38] Hsu, M.-C., Akkerman, I., and Bazilevs, Y., 2012, "Wind Turbine Aerodynamics Using ALE–VMS: Validation and the Role of Weakly Enforced Boundary Conditions," Comput. Mech., **50**(4), pp. 499–511.

[39] Kiendl, J., Bletzinger, K.-U., Linhard, J., and Wüchner, R., 2009, "Isogeometric Shell Analysis With Kirchhoff–Love Elements," Comput. Methods Appl. Mech. Eng., **198**(49–52), pp. 3902–3914.

[40] Raknes, S., Deng, X., Bazilevs, Y., Benson, D., Mathisen, K., and Kvamsdal, T., 2013, "Isogeometric Rotation-Free Bending-Stabilized Cables: Statics, Dynamics, Bending Strips and Coupling With Shells," Comput. Methods Appl. Mech. Eng., **263**, pp. 127–143.

[41] Hughes, T. J. R., Cottrell, J. A., and Bazilevs, Y., 2005, "Isogeometric Analysis: CAD, Finite Elements, NURBS, Exact Geometry, and Mesh Refinement," Comput. Methods Appl. Mech. Eng., **194**(39–41), pp. 4135–4195.

[42] Cottrell, J. A., Hughes, T. J. R., and Bazilevs, Y., 2009, *Isogeometric Analysis: Toward Integration of CAD and FEA*, Wiley, Chichester, UK.

[43] Tezduyar, T. E., and Sathe, S., 2007, "Modeling of Fluid–Structure Interactions With the Space–Time Finite Elements: Solution Techniques," Int. J. Numer. Methods Fluids, **54**(6–8), pp. 855–900.

[44] Tezduyar, T. E., Sathe, S., Pausewang, J., Schwaab, M., Christopher, J., and Crabtree, J., 2008, "Interface Projection Techniques for Fluid–Structure Interaction Modeling With Moving-Mesh Methods," Comput. Mech., **43**(1), pp. 39–49.

[45] Tezduyar, T. E., Schwaab, M., and Sathe, S., 2009, "Sequentially-Coupled Arterial Fluid–Structure Interaction (SCAFSI) Technique," Comput. Methods Appl. Mech. Eng., **198**(45–46), pp. 3524–3533.

[46] Takizawa, K., Christopher, J., Tezduyar, T. E., and Sathe, S., 2010, "Space–Time Finite Element Computation of Arterial Fluid–Structure Interactions With Patient-Specific Data," Int. J. Numerical Methods Biomed. Eng., **26**(1), pp. 101–116.

[47] Tezduyar, T. E., Takizawa, K., Moorman, C., Wright, S., and Christopher, J., 2010, "Multiscale Sequentially-Coupled Arterial FSI Technique," Comput. Mech., **46**(1), pp. 17–29.

[48] Tezduyar, T. E., Takizawa, K., Moorman, C., Wright, S., and Christopher, J., 2010, "Space–Time Finite Element Computation of Complex Fluid–Structure Interactions," Int. J. Numer. Methods Fluids, **64**(10–12), pp. 1201–1218.

[49] Takizawa, K., Moorman, C., Wright, S., Purdue, J., McPhail, T., Chen, P. R., Warren, J., and Tezduyar, T. E., 2011, "Patient-Specific Arterial Fluid–Structure Interaction Modeling of Cerebral Aneurysms," Int. J. Numer. Methods Fluids, **65**(1–3), pp. 308–323.

[50] Takizawa, K., and Tezduyar, T. E., 2011, "Multiscale Space–Time Fluid–Structure Interaction Techniques," Comput. Mech., **48**(3), pp. 247–267.

[51] Tezduyar, T. E., Takizawa, K., Brummer, T., and Chen, P. R., 2011, "Space–Time Fluid–Structure Interaction Modeling of Patient-Specific Cerebral Aneurysms," Int. J. Numer. Methods Biomed. Eng., **27**(11), pp. 1665–1710.

[52] Takizawa, K., and Tezduyar, T. E., 2012, "Space–Time Fluid–Structure Interaction Methods," Math. Models Methods Appl. Sci., **22**(Supp 02), p. 1230001.

[53] Bazilevs, Y., and Hughes, T. J. R., 2008, "NURBS-Based Isogeometric Analysis for the Computation of Flows About Rotating Components," Comput. Mech., **43**(1), pp. 143–150.

[54] Tezduyar, T., Aliabadi, S., Behr, M., Johnson, A., Kalro, V., and Litke, M., 1996, "Flow Simulation and High Performance Computing," Comput. Mech., **18**(6), pp. 397–412.

[55] Behr, M., and Tezduyar, T., 1999, "The Shear-Slip Mesh Update Method," Comput. Methods Appl. Mech. Eng., **174**(3–4), pp. 261–274.

[56] Behr, M., and Tezduyar, T., 2001, "Shear-Slip Mesh Update in 3D Computation of Complex Flow Problems With Rotating Mechanical Components," Comput. Methods Appl. Mech. Eng., **190**(24–25), pp. 3189–3200.
[57] Tezduyar, T. E., 2001, "Finite Element Methods for Flow Problems With Moving Boundaries and Interfaces," Arch. Comput. Methods Eng., **8**(2), pp. 83–130.
[58] Tezduyar, T. E., 2007, "Finite Elements in Fluids: Special Methods and Enhanced Solution Techniques," Comput. Fluids, **36**(2), pp. 207–223.
[59] Takizawa, K., Tezduyar, T. E., and Kostov, N., 2014, "Sequentially-Coupled Space-Time FSI Analysis of Bio-Inspired Flapping-Wing Aerodynamics of an MAV," Comput. Mech., February (published online).
[60] Takizawa, K., 2014, "Computational Engineering Analysis With the New-Generation Space-Time Methods," Comput. Mech., March (published online).
[61] Takizawa, K., Tezduyar, T. E., Buscher, A., and Asada, S., 2014, "Space-Time Interface-Tracking With Topology Change (ST-TC)," Comput. Mech., October (published online).
[62] Takizawa, K., and Tezduyar, T. E., 2014, "Space–Time Computation Techniques With Continuous Representation in Time (ST-C)," Comput. Mech., **53**(1), pp. 91–99.
[63] Takizawa, K., Tezduyar, T. E., Boben, J., Kostov, N., Boswell, C., and Buscher, A., 2013, "Fluid–Structure Interaction Modeling of Clusters of Spacecraft Parachutes With Modified Geometric Porosity," Comput. Mech., **52**(6), pp. 1351–1364.
[64] Tezduyar, T. E., Behr, M., Mittal, S., and Johnson, A. A., 1992, "Computation of Unsteady Incompressible Flows With the Finite Element Methods—Space–Time Formulations, Iterative Strategies and Massively Parallel Implementations," New Methods in Transient Analysis, PVP-Vol. 246/AMD-Vol. 143, ASME, pp. 7–24.
[65] Tezduyar, T., Aliabadi, S., Behr, M., Johnson, A., and Mittal, S., 1993, "Parallel Finite-Element Computation of 3D Flows," Computer, **26**(10), pp. 27–36.
[66] Johnson, A. A., and Tezduyar, T. E., 1994, "Mesh Update Strategies in Parallel Finite Element Computations of Flow Problems With Moving Boundaries and Interfaces," Comput. Methods Appl. Mech. Eng., **119**(1–2), pp. 73–94.
[67] Stein, K., Tezduyar, T., and Benney, R., 2003, "Mesh Moving Techniques for Fluid–Structure Interactions With Large Displacements," ASME J. Appl. Mech., **70**(1), pp. 58–63.
[68] Karypis, G., and Kumar, V., 1999, "A Fast and High Quality Multilevel Scheme for Partitioning Irregular Graphs," SIAM J. Sci. Comput., **20**(1), pp. 359–392.
[69] Bazilevs, Y., Hsu, M. C., and Bement, M. T., 2013, "Adjoint-Based Control of Fluid–Structure Interaction for Computational Steering Applications," Proc. Comput. Sci., **18**, pp. 1989–1998.
[70] Texas Advanced Computing Center (TACC) 2013, University of Texas, Austin, TX, http://www.tacc.utexas.edu